GSA Data Repository 2018035

Leydet et al., 2018, Opening of glacial Lake Agassiz's eastern outlets by the start of the Younger Dryas cold period: Geology, https://doi.org/10.1130/G39501.1.

METHODS

Geomorphic setting and field methods. The overall study area encompasses the region surrounding Thunder Bay, Ontario. Four sites were selected based on work that previously defined the eastern outlet channels of the glacial Lake Agassiz drainage basin based on paleotopography and channel presence (Teller et al., 2005; Breckenridge, 2015). We sampled boulders from topographically stable positions on bedrock highs around the North Lake channel, Flatrock Lake channel, and Lake Kaministiquia (Kam) channels (Fig. 2). The Lake Kam region encompasses several sub-outlets that all route through our sampling area (Fig. 2). The Steep Rock moraine separates the North Lake and Flatrock Lake channels; The Brule moraine separates the Flatrock Lake channel from the Lake Kam channels (Fig. 2). We also sampled south of Lake Nipigon behind the Marks moraine (Fig. 2). We purposely sampled on bedrock highs located above outlet channels to avoid areas that may have been disturbed by meltwater. In the case of Lake Kam, we made sure to sample above this proglacial lake that formed at the end of the Younger Dryas when the Laurentide ice sheet deposited the Marks moraine blocking eastward Lake Agassiz basin routing into Lake Superior (Lowell et al., 1999; Teller et al., 2005; Breckenridge, 2015). Our sample locations on bedrock highs minimize possible exhumation of boulders from sediment that can occur on moraines, which would reduce the deglaciation age. By sampling high points on the terrain, we also reduce the potential for snow cover affecting *in situ* cosmogenic nuclide production, because the areas are windswept (Gosse and Phillips, 2001). Boulder samples have no topographic shielding. Two to four kg of sample were removed using a hammer and chisel on the top surface of the boulder. Latitude, longitude, and elevation were recorded for each sample (Table DR1).

Sample processing and analytical techniques. All samples were prepared at Oregon State University's Cosmogenic Nuclide Laboratory. In order to physically isolate quartz, bulk rock samples were crushed, pulverized, and sieved down to a 250-500 μm fraction. Physical separation continued with magnetic separation of magnetic and non-magnetic minerals. Chemical separation of quartz was performed by frothing the sample using a laurel amine, compressed CO_2, and deionized water solution, followed by etching in dilute HF/HNO_3. Quartz purity was tested at the University of Colorado-Boulder. A known concentration and amount of the low-^{10}Be OSU-Blue Be carrier was added to each sample (Murray et al., 2012). Samples were converted to BeO through dissolution, anion and cation exchange, precipitation, and oxidizing steps. ^{10}Be/^{9}Be ratios were measured by accelerator mass spectrometry (AMS) at Purdue University's Rare Isotope Measurement Laboratory (PRIME) against the 07KNSTD standard. Blanks averaged ~1.17×10^{-15} ^{10}Be/^{9}Be (n=4).

Exposure age calculation. Following Cuzzone et al. (2016) and Ullman et al. (2016), we quantify the time-varying effects of uplift and atmospheric pressure on the ^{10}Be production rates since exposure of our sites. We apply an isostatic surface loading model (Mitrovica et al., 1994) that includes the influence of ice loading, using the ICE-5G reconstruction of ice thickness and its partnering Earth viscosity model, VM2 (Peltier, 2004), ocean loading (Mitrovica and Milne, 2003) and variations in Earth rotation (Mitrovica et al., 2005) to estimate changes in altitude for each site. This approach explicitly estimates the true vertical land motion, without the confounding effects of global-mean sea-level rise and the gravitational attraction of the remaining ice sheets.

We use output from an atmospheric-ocean general circulation model providing simulated climate at 3 ka time slices from 21 ka to 0 ka (Alder and Hostetler, 2015) to determine the changes in atmospheric pressure (Stone, 2000; Staiger et al., 2007). We linearly interpolate this output between simulations to estimate the change in atmospheric thickness due to the change in surface air pressure using the hypsometric equation (Cuzzone et al., 2016; Ullman et al., 2016). Through this method, we determine the elevation correction for our sites that range from 6 m to 15 m. While opposing the uplift correction in direction, this small atmospheric correction does not offset the uplift correction in magnitude. In addition, the atmospheric correction is within the accuracy of our site measurement of altitude. Therefore, we exclude the atmospheric correction in our overall sample correction and only account for the topographic uplift in our age estimates.

Sample ages were calculated using the CRONUS-Earth Calculator version 2.2 with the Northeast North America (NENA) production rate (Balco et al., 2009) (Table DR1); we use this version as it allows the use of a regional production rate from close to our study area (later versions do not allow the use of regional production rate calibrations). Note that this production rate does not include an uplift or atmospheric correction. Similar to our findings, Balco et al. (2009) deemed atmospheric changes to be minimal following Staiger et al. (2007). Balco et al. (2009) also calculated the effect of including uplift on the production rate in the same manner as we have for our samples and found its effect to be 1.5-2.5%, which is within the uncertainty of the production rate. As such, this uncorrected-production rate is applicable to our uplift-corrected samples. The reason for the difference in uplift effects is that our sample sites are from the interior of the Laurentide ice sheet whereas the production-rate sites are from near the Laurentide ice-sheet maximum margin along the eastern seaboard of North America where ice was significantly thinner and covered the sites for a shorter period of time. Several studies have shown the NENA production rate to be applicable to our sites where independent age control is available. Ullman et al. (2016) dated the Sakami Moraine in western Quebec that formed upon the opening of Hudson Bay. Only using the NENA production rate with the uplift correction for the Sakami samples does the moraine ^{10}Be age agree with the independent constraints on the moraine age of ~8.2 ka (Hillaire-Marcel et al., 1981; Barber et al., 1999). Likewise, ^{14}C age constraints on a Tiedemann Glacier moraine in British Columbia agree with ^{10}Be ages from the moraine using the NENA production rate (Menounos et al., 2013). Thus, the NENA production rate is applicable to our study region that lies in southern Canada between these two independent confirmation sites.

We analyze our data based on the Lal/Stone time-dependent scheme along with the internal uncertainty (Table DR1). Uncertainty in the production rate is 4.8% (Balco et al., 2009). Utilizing other scaling schemes (Balco et al., 2009) or production rates (Lifton et al., 2015) does not alter our conclusions as the ages are within the internal uncertainty of our reported ages (Table DR2).

Removal of outliers and calculation of site averages. We find six outliers (with a potential seventh – see text) out of our 23 samples (Fig. DR1). North Lake's outlier (n=1) is a young age (NL-4-15) that disagrees with the minimum-limiting ^{14}C age of deglaciation of 12.5±0.1 ka (Lowell et al., 2009). This sample was also the smallest boulder we sampled. We interpret this young age as reflecting post-depositional movement or exhumation from a thin till cover that used to rest on the bedrock. Flatrock Lake has two samples that are younger than the minimum-limiting ^{14}C age of deglaciation of 12.3±0.2 ka (Lowell et al., 2009), also reflecting potential exhumation. The Lake Kam outliers (n=2) are either too old or too young based on the most basic understanding of Laurentide ice-sheet deglaciation in this region (Teller et al., 2005, Lowell et al., 2009; Breckenridge, 2015). Specifically, the old age is out of stratigraphic order with even the North Lake ages and may contain inheritance. The young age disagrees with the minimum-limiting ^{14}C age of deglaciation of 12.0±0.2 ka (Lowell et al., 2009) and thus may have been exhumed following deposition. In addition, these two ages are statistical outliers based on Grubb's criteria for testing outliers from a normally distributed population (Komsta, 2011); $p=0.007827$. There is a third potential young outlier, who's inclusion or exclusion does not affect our conclusions (see text). Our site behind the Marks moraine has one old outlier that is out of stratigraphic order with retreat from the Marks moraine post-dating the end of the Younger Dryas (Teller et al., 2005), suggesting that it contains some inheritance. Inclusion of the one old sample results in a mean of 11.7±0.5 ka, which does not change our conclusions. We calculated an arithmetic mean and standard error for each of our study sites as the best estimate for the timing of Laurentide ice-sheet retreat from the outlet (Bevington and Robinson, 2002). We use the standard error of the mean as this is a more conservative assessment our sample uncertainty; the uncertainty from an error-weighted mean (the mean is the same by either approaches) is less than the approach we use. In Figure DR2, we test our removal of outliers with quantile-quantile plots (Ullman et al., 2016) to show the normality of the final samples used to calculate the mean and its uncertainty.

REFERENCES CITED

Alder, J.R., and Hostetler, S.W., 2015, Global climate simulations at 3000-yr intervals for the last 21,000 years with the GENMOM coupled atmosphere-ocean model: Climate of the Past, v. 11, p. 449-171.

Balco, G., Briner, J., Finkel, R.C., Rayburn, J.A., Ridge, J.C., and Schaefer, J.M., 2009, Regional beryllium-10 production rate calibration for northeastern North America: Quaternary Geochronology, v. 4, p. 93-107.

Barber, D.C., Dyke, A., Hillaire-Marcel, C., Jennings, A.E., Andrews, J.T., Kerwin, M.W., Bilodeau, G., McNeely, R., Southon, J., Morehead, M.D., and Gagnon, J.-M., 1999, Forcing of the cold event of 8,200 years ago by catastrophic drainage of Laurentide lakes: Nature, v. 400, p. 344-348.

Bevington, P., and Robinson, D.K., 2002, Data Reduction and Error Analysis for the Physical Sciences, 3rd Ed.: McGraw-Hill, 336 pp.

Breckenridge, A., 2015, The Tintah-Campbell gap and implications for glacial Lake Agassiz drainage during the Younger Dryas cold interval: Quaternary Science Reviews, v. 117, p. 124-134.

Cuzzone, J.K., Clark, P.U., Carlson, A.E., Ullman, D.J., Rinterknecht, V.R., Milne, G.A., Pekka, J., Wohlfarth, B., Marcott, S.A., and Caffee, M., 2016, Final deglaciation of the Scandinavian Ice Sheet and implications for the Holocene global sea-level budget: Earth and Planetary Science Letters, v. 448, p. 34-41.

Gosse, J.C., and Phillips, F.M., 2001, Terrestrial in situ cosmogenic nuclides: theory and application: Quaternary Science Reviews, v. 20, p. 1475-1560.

Hillaire-Marcel, C., Occhietti, S., and Vincent, J.-S., 1981, Sakami moraine, Quebec: A 500-km-long moraine without climatic control: Geology, v. 9, p. 210-214.

Komsta, L., 2011, Outliers: Tests for outliers: R package version 0.14, https://CRAN.R-project.org/package=outliers.

Lifton, N., Caffee, M., Finkel, R., Marrero, S., Nishiizumi, K., Phillips, F.M., Goehring, B., Gosse, J., Stone, J., Schaefer, J., Theriault, B., Jull, A.J.T., and Fifield, K., 2015, In situ cosmogenic nuclide production rate calibration for the CRONUS-Earth project from Lake Bonneville, Utah, shoreline features: Quaternary Geochronology, v. 26, p. 56-69.

Lowell T.V., Fisher, T.G., Hajdas, I., Glover, K., Loope, H., and Henry, T., 2009, Radiocarbon deglaciation chronology of the Thunder Bay, Ontario area and implications for ice sheet retreat patterns: Quaternary Science Reviews, v. 28, p. 1597-1607.

Lowell T.V., Larson G.J., Hughes J.D., and Denton G.H., 1999, Age verification of the Lake Gribben forest bed and the Younger Dryas advance of the Laurentide Ice Sheet: Canadian Journal of Earth Science, v. 36, p. 383-393.

Menounos B., Clague, J.J., Clarke, G.K.C., Marcott, S.A., Osborn, G., Clark, P.U., Tennant, C., and Novak, A.M., 2013, Did rock avalanche deposits modulate the late Holocene advance of Tiedemann Glacier, southern Coast Mountains, British Columbia, Canada?: Earth and Planetary Science Letters, v. 384, p. 154-164.

Mitrovica, J.X., and Milne, G.A., 2003, On post-glacial sea level: I General theory: Geophysical Journal International: v. 154, p. 253-267.

Mitrovica, J.X., Davis, J.L., and Shapiro, I.I., 1994, A Spectral Formalism for Computing 3-Dimensial Deformations Due to Surface Loads: 1. Theory: Journal of Geophysical Research, v. 99, p. 7057-7073.

Mitrovica, J.X., Wahr, J., Matsuyama, I., and Paulson, A., 2005, The rotational stability of the ice-age earth: Geophysical Journal International, v. 161, p. 491-506.

Murray, D.S., Carlson, A.E., Singer, B.S., Anslow, F.S., He, F., Caffee, M., Marcott, S.A., Liu, Z., and Otto-Bliesner, B.L., 2012, Northern Hemisphere forcing of the last deglaciation in southern Patagonia: Geology, v. 40, p. 631-634.

Peltier, W.R., 2004, Global glacial isostasy and the surface of the ice-age earth: The ICE-5G (VM2) model and GRACE: Annual Review of Earth and Planetary Sciences, v. 32, p. 111-149.

Rasmussen, S.O., Andersen, K.K., Svensson, A.M., Steffensen, J.P., Vinther, B.M., Clausen, H.B., Siggaard-Andersen, M.-L., Johnsen, S.J., Larsen, L.B., Dahl-Jensen, D., Bigler, M., Röthlisberger, Fischer, H., Goto-Azuma, K., Hansson, M.E., and Ruth, U., 2006, A new Greenland ice core chronology for the last glacial termination: Journal of Geophysical Research, v. 111, doi: 10.1029/2005JD006079.

Staiger, J., Gosse, J., Toracinta, R., Oglesby, B., Fastook, J., and Johnson, J.V., 2007, Atmospheric scaling of cosmogenic nuclide production: Climate effect: Journal of Geophysical Research, v. 112, doi: 10.1029/2005JB003811.

Stone, J.O., 2000, Air pressure and cosmogenica isotope production. Journal of Geophysical Research, v. 105, p. 23,753-23,759.

Teller, J. T., Boyd, M., Yang, Z., Kor, P.S.G., and Fard, A.M., 2005, Alternative routing of Lake Agassiz overflow during the Younger Dryas: new dates, paleotopography, and a re-evaluation: Quaternary Science Reviews, v. 24, p. 1890-1905.

Ullman, D.J., Carlson, A.E., Hostetler, S.W., Clark, P.U., Cuzzone, J.K., Milne, G.A., Winsor, K., and Caffee, M., 2016, Final deglaciation of the Laurentide ice sheet in the early to middle Holocene: Quaternary Science Review, v. 152, p. 49-59.

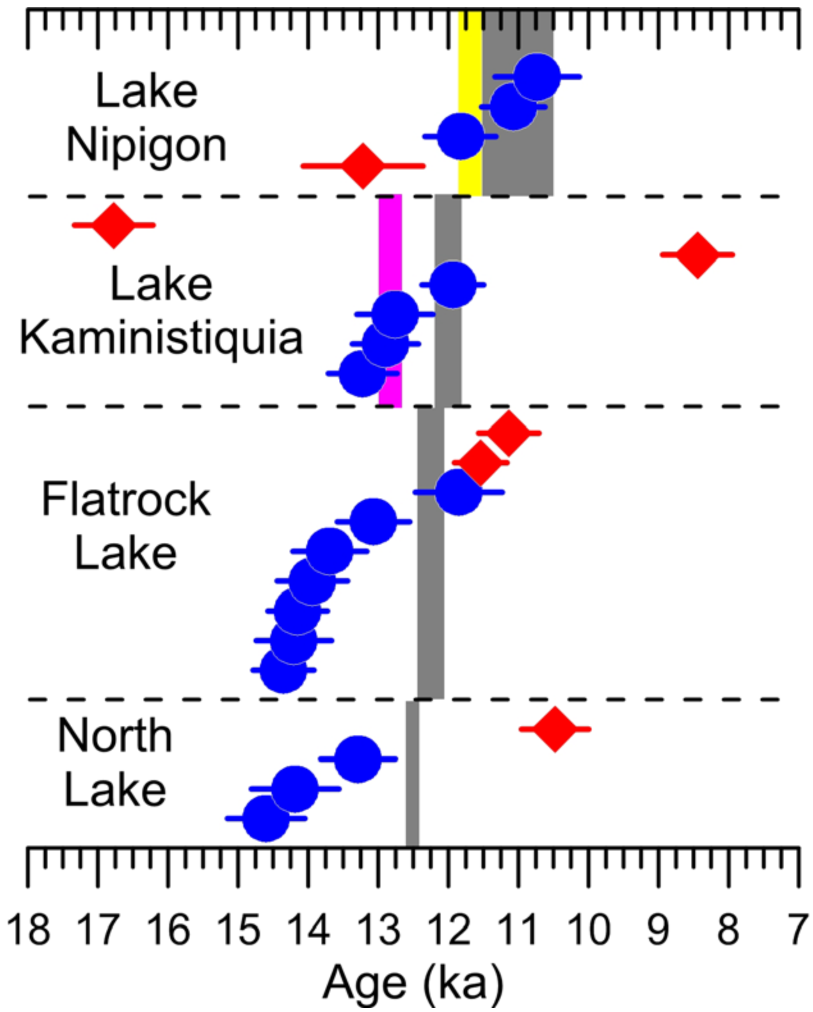

Figure DR1. ^{10}Be ages with outliers denoted by red diamonds. Bars are 1-σ uncertainty. Gray bars are minimum-limiting ^{14}C age constraints on the outlets (Lowell et al., 2009) used to identify outliers. Purple bar is the start of the Younger Dryas; yellow bar is the end of the Younger Dryas (Rasmussen et al., 2006).

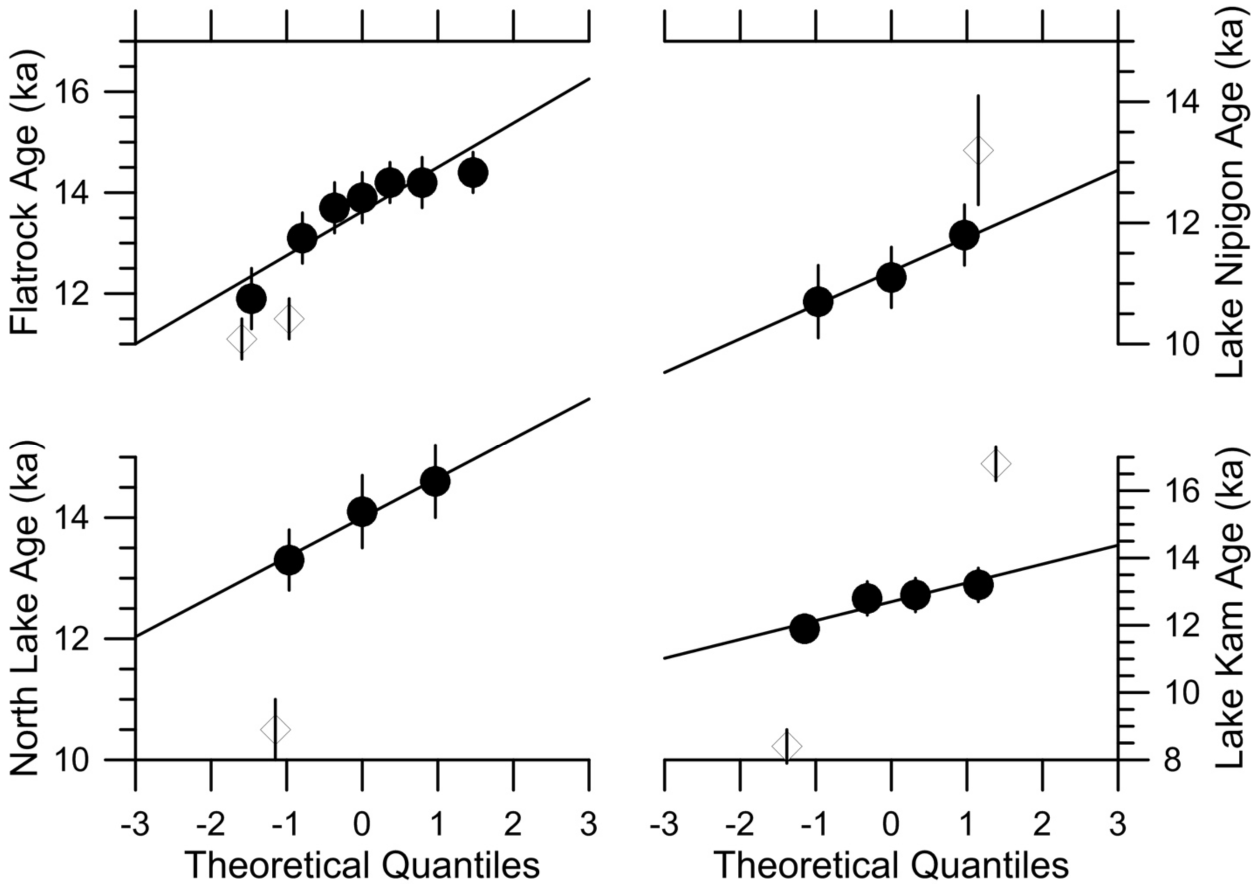

Figure DR2. Exposure age versus theoretical quantile for each of the sample groupings (Ullman et al., 2016). This modified version of a Quantile-Quantile plot includes the internal uncertainty for each of the dates. The black line on each plot shows the expected result for a normal distribution (scaled with the mean and standard deviation of each sample grouping). Solid circles are the ages used to calculate the mean; open diamonds are the excluded outlier samples.

Table DR1. Cosmogenic Surface Exposure Ages for the Eastern Outlets by sample site

Sample	Latitude	Longitude	Modern Elevation (m asl)	Corrected Elevation (m)[d]	Thickness (cm)	Quartz (g)	^{9}Be Mass added (g)	^{10}Be/^{9}Be ratio (10^{-15})	Internal Uncertainty (10^{-15})	^{10}Be (atoms g^{-1})[e]	Uncertainty (atoms g^{-1})	^{10}Be age (ka)[b, c]
North Lake Site												
NL-1-15	48.046	-90.045	517	455	3.5	44.1627	0.8751	185.14	6.33	87455	3318	14.6 ± 0.6
NL-3-15	48.052	-90.047	475	413	4	44.8610	0.8746	164.02	5.94	76499	3079	13.3 ± 0.5
NL-4-15*	48.056	-90.054	466	404	2	50.3218	0.8784	145.55	6.03	60778	2798	10.5 ± 0.5
NL-5-15	48.056	-90.054	462	400	2	43.6625	0.8729	171.69	6.83	81799	3612	14.1 ± 0.6
											Site Mean Age[a]	**14.0 ± 0.4**
Flat Rock Site												
FR-1-15	48.293	-90.266	490	424	3	40.0132	0.8736	159.91	4.33	83181	2504	14.2 ± 0.4
FR-2-15	48.293	-90.266	490	424	2.5	37.6572	0.8780	148.53	4.79	82192	2975	13.9 ± 0.5
FR-4-15*	48.292	-90.265	492	426	2.5	35.3228	0.8743	112.23	3.86	65761	2554	11.1 ± 0.4
FR-5-15*	48.291	-90.266	495	429	2	51.6664	0.8748	170.14	4.99	68653	2238	11.5 ± 0.4
FR-6-15	48.291	-90.266	496	430	3	53.7861	0.8720	218.32	7.39	83877	3184	14.2 ± 0.5
FR-7-15	48.291	-90.266	498	432	2	35.3071	0.8663	122.41	5.68	70636	3718	11.9 ± 0.6
FR-8-15	48.285	-90.265	511	445	2	46.8733	0.8775	177.16	6.29	78818	3130	13.1 ± 0.5
FR-9-15	48.284	-90.265	512	446	1.5	35.8776	0.8714	143.63	4.99	83076	3212	13.7 ± 0.5
FR-11-15	48.284	-90.265	506	440	1	59.3766	0.8677	250.66	6.79	86909	2641	14.4 ± 0.4
											Site Mean Age[a]	**13.6 ± 0.3**
Lake Kam Outlet Site												
KM-1-15	48.528	-89.664	494	426	2	52.0606	0.8751	196.62	6.57	78592	2931	13.2 ± 0.5
KM-3-15*	48.528	-89.665	484	416	3.5	23.2368	0.8788	55.51	2.86	49169	2919	8.4 ± 0.5
KM-4-15	48.529	-89.667	475	407	3	39.8282	0.8752	143.21	4.74	74941	2756	12.9 ± 0.5
KM-5-15	48.527	-89.665	487	419	3	52.0729	0.8643	178.15	5.88	69914	2599	11.9 ± 0.4
KM-7-15*	48.527	-89.665	487	419	3	46.9759	0.8801	220.74	6.63	98411	3299	16.8 ± 0.5
KM-9-15	48.522	-89.662	479	411	2	41.8971	0.8757	150.69	5.80	75022	3210	12.8 ± 0.5
											Site Mean Age[a]	**12.7 ± 0.3**
Lake Nipigon Site												
LN-8-15*	48.704	-88.627	280	213	1	47.2033	0.8639	149.36	8.76	65104	4244	13.2 ± 0.9
LN-10-15	48.704	-88.627	282	215	2.5	46.6695	0.8688	121.90	4.52	53995	2227	11.1 ± 0.5
LN-11-15	48.704	-88.628	271	204	3	31.0688	0.8785	76.08	3.86	51464	2915	10.7 ± 0.6
LN-12-15	48.704	-88.628	271	204	4	46.6124	0.8611	129.41	4.92	56275	2432	11.8 ± 0.5
											Site Mean Age[a]	**11.2 ± 0.3**

* Denotes Outliers excluded from error weighted mean calculation

[a] Site mean age calculates using error weighted mean

[b] Lal/Stone Time Dependent scaling scheme ages presented from the CRONUS Earth online calculator v. 2.2

[c] Ages calculated with standard atmosphere, no shielding, density of 2.65 g cm^{3}, and erosion of 0

[d] Elevations are uplift corrected (see text)

[e] Be atom concentrations are blank corrected (see text)

Table DR2. Cosmogenic Surface Exposure Ages by production rate and scaling scheme

Sample	Internal Uncertainty (yr)	Lifton (yr)	External Uncertainty (yr)	Lal/Stone (yr)	External Uncertainty (yr)
North Lake Site					
NL-1-15	551	14362	890	14559	898
NL-3-15	503	13125	832	13289	839
NL-4-15*	453	10349	695	10477	701
NL-5-15	622	13966	921	14148	930
Site Mean (ka)		**13.8 ± 0.4**		**14.0 ± 0.4**	
Flat Rock Site					
FR-1-15	424	13966	802	14163	810
FR-2-15	473	13748	837	13940	845
FR-4-15*	405	10994	687	11137	693
FR-5-15*	374	11403	670	11549	676
FR-6-15	537	14005	868	14204	876
FR-7-15	620	11701	841	11851	850
FR-8-15	486	12893	813	13068	820
FR-9-15	527	13514	843	13703	851
FR-11-15	434	14148	815	14352	823
Site Mean (ka)		**13.4 ± 0.3**		**13.6 ± 0.3**	
Lake Kam Outlet Site					
KM-1-15	461	13033	802	13222	810
KM-3-15*	467	8292	638	8445	648
KM-4-15	472	12751	781	12933	788
KM-5-15	440	11773	723	11936	730
KM-7-15*	527	16478	978	16774	991
KM-9-15	544	12619	821	12798	829
Site Mean (ka)		**12.5 ± 0.3**		**12.7 ± 0.3**	
Lake Nipigon Site					
LN-8-15*	856	13014	1062	13241	1078
LN-10-15	453	10910	698	11096	707
LN-11-15	564	10546	790	10732	801
LN-12-15	506	11630	759	11828	769
Site Mean (ka)		**11.0 ± 0.3**		**11.2 ± 0.3**	

* Denotes outliers not included in site mean calculations